Astron. Astrophys. 343, 536–544 (1999)

ASTRONOMY
AND
ASTROPHYSICS

Spatially resolved nebulae around the Ofpe/WN9 stars S 61 and BE 381⋆

A. Pasquali[1], **A. Nota**[2,⋆⋆], **and M. Clampin**[2]

[1] ST-ECF/ESO, Karl-Schwarzschild-Strasse 2, D-85748 Garching bei München, Germany (apasqual@eso.org)
[2] Space Telescope Science Institute, 3700 San Martin Drive, Baltimore, MD 21218, USA (nota@stsci.edu; clampin@stsci.edu)

Received 21 August 1998 / Accepted 27 October 1998

Abstract. We present new high-resolution coronographic imaging and medium-resolution spectroscopy of the circumstellar region around S 61 and BE 381, two Ofpe/WN9 stars in the Large Magellanic Cloud. The observations were carried out at the ESO/NTT (La Silla) in January 1996 and July 1998. The excellent seeing conditions allowed the circumstellar nebulae associated with both S 61 and BE 381 to be spatially resolved for the first time. The nebula surrounding S 61 has the appearance of a shell with a mild central axisymmetry. The surface brightness is not uniform, and the northern region of the nebula is the brightest. The nebula exhibits a bipolar structure with an overall morphology very similar to nebulae around other LBVs or Opfe/WN9 stars, especially S119. The diameter of the shell is 7.3″, corresponding to a linear size of 1.8 pc. From the profile of nebular emission lines we clearly detect an expansion motion with a velocity of 28 km s^{-1}, which indicates a dynamical age of $\sim$ 30000 yrs. We find an electron density of 400 cm^{-3} and an electron temperature of 6120 K. The nebula is similar to other LBV nebulae in that it is nitrogen enriched. The observed chemical and dynamical properties confirm that the nebula is associated with the central star and is of stellar origin. This result implies that S 61 is likely to have undergone a LBV-type ouburst and, therefore, strenghtens the suggestion that Ofpe/WN9 stars are quiescent LBVs. The situation is different for BE 381. The Hα images of BE 381 also reveal the presence of a faint nebulosity around the star; most of the nebular flux appears to be emitted by an arc of gas located to the east of BE 381, while a much dimmer arc is detectable on the western side. The arcs delineate a shell of 13″ in diameter, corresponding to a linear size of 3.2 pc, which appears to be expanding with a velocity of 14 km s^{-1}. From the nebular emission lines we derive an electron density ranging between 30 cm^{-3} and 120 cm^{-3} (assuming T_e = 10000 K), and a N^+/S^+ ratio between 1.5 and 2.3, which are typical of HII regions. We therefore conclude that the shell detected around BE 381 is not of stellar origin and probably represents the relic of the interstellar bubble blown by BE 381 during its O main-sequence phase.

Key words: stars: circumstellar matter – stars: emission-line, Be – stars: individual: BE 381 LMC – stars: individual: S 61 LMC – stars: supergiants

1. Introduction

Ofpe/WN9 stars have only recently received wide-spread attention, but are now central to understanding the evolution of massive stars. The Ofpe/WN9 class was first introduced by Walborn (1982), who discovered several Of-like objects with very extended envelopes and, in order to indicate that these stars could neither be classified as pure WNL stars, nor as pure Of stars, introduced the Ofpe/WN9 classification. The presence of nebular lines indicated enhanced nitrogen abundances, suggesting that the circumstellar gas had been ejected by the stars during their post main sequence evolution. Bohannan & Walborn (1989) subsequently summarized the properties of all known Ofpe/WN9 stars in the Large Magellanic Cloud (LMC).

The significance of Ofpe/WN9 stars was first recognized when Stahl et al. (1983) discovered that the prototype of the Ofpe/WN9 class (R127) had turned into a Luminous Blue Variable (LBV) on a timescale of less than a few years. Stahl (1986) also found that when the bright LBV AG Carinae is in a high-temperature state, it displays the spectral characteristics of Ofpe/WN9 stars. LBVs as a class were introduced by Conti (1984), although some of them had already been studied individually four decades ago (Hubble & Sandage 1953). Together with the Ofpe/WN9 stars, LBVs populate the uppermost part of the HR Diagram, and are believed to be in evolutionary transition to Wolf-Rayet stars (Maeder 1989). LBV evolution is characterized by enhanced mass-loss rates, outbursts and shell ejections. Observationally, LBVs display irregular photometric (0.5–2 mag) and spectral variations over timescales of decades. In addition, they sometimes undergo *"giant outbursts"*, in which they eject a significant fraction of their mass. The ejected mass is often observed in the form of a spectacular circumstellar nebula (e.g. η Car, Davidson 1987).

The observational evidence indicates that there is a close relationship between the class of LBVs and the Ofpe/WN9 stars. The possibility of such a relationship has been investigated by Smith, Crowther & Prinja (1994), who proposed that

Send offprint requests to: A. Pasquali

⋆ Based on observations obtained at the European Southern Observatory, La Silla, Chile

⋆⋆ Affiliated with the Astrophysics Division, Space Science Department of the European Space Agency

some LBVs show spectral morphologies that make them appear as an extension of the WN sequence towards later spectral types, hence unifying the classes of WNL, LBV and Ofpe/WN9 stars. Recently, Nota et al. (1996b) presented a new dataset comprising ground-based, high S/N echelle spectra of the complete sample of Ofpe/WN9, with two Of and B[e] stars taken for comparison. They concluded, on the basis of the spectral morphologies alone, that the Ofpe/WN9 type formed a very homogeneous group, with wind characteristics in between the Of and the B[e] stars. At the same time, Morris et al. (1996) independently reached the same conclusion on the *transitional* nature of Ofpe/WN9 and LBVs, by comparing IR spectra of Ofpe/WN9, LBVs late-type WN stars and B[e]. Pasquali et al. (1997) and Crowther et al. (1995) finally placed these statements on a firm quantitative footing by deriving the fundamental parameters of these stars. Pasquali et al. (1997) used ultraviolet HST/FOS spectra for the same sample of Ofpe/WN9 stars studied by Nota et al. (1996b), and investigated the evolutionary status of these stars, concluding that most likely the Ofpe/WN9 stars are quiescent LBVs.

This concept had already been proposed by Nota et al. (1996), on the basis that, although Ofpe/WN9 stars do not display any variability, in some cases they show an associated circumstellar nebula which is most likely the relic of a LBV-type outburst which occurred some time in their post main sequence evolutionary history. Out of the seven Ofpe/WN9 stars they considered, they found that five showed evidence of nebular emission lines in their spectra, confirming the original findings by Walborn (1982). Unfortunately, the high resolution echelle spectra used for their investigation did not provide sufficient spatial information to study in detail the characteristics of the detected nebular emission, except for S119. The nebula around S119 was subsequently imaged (Nota et al. 1994; Smith et al. 1998), and was found to have morphological and physical properties very similar to most LBV nebulae. The nebula was most likely ejected by the central star $\simeq 5 \times 10^4$ yrs ago.

In order to further investigate the relationship between LBVs and Ofpe/WN9 stars, we have initiated a program of high resolution coronographic imaging and medium resolution longslit spectroscopy of the circumstellar environment of all Ofpe/WN9 stars displaying presence of nebular lines in their spectra. Our objective is threefold: 1) to establish the presence of a circumstellar nebula, 2) to assess whether the nebula is physically associated with the star, 3) to study in detail the kinematical and chemical properties of the resolved Ofpe/WN9 nebulae and compare them to known LBV nebulae, to strengthen the suspected connection between the two classes of objects.

2. The data

2.1. Observations and observation strategy

We observed BE 381 and S 61 at the 3.5m ESO/NTT telescope (La Silla, Chile), on the nights of January 26–28, 1996 and July 31, 1998, using the STScI Coronograph mounted at the SUSI focal plane, and the EMMI spectrograph in Red Medium Dispersion (REMD) and Blue Medium Dispersion (BLMD). The journal of both coronographic and spectroscopic observations is given in Table 1. The NTT/STScI coronograph is described in detail in Clampin et al. (1994). The coronographic images were taken using an occulting bar of 3.5″, in the light of Hα (λ_c = 6562.7 Å, FWHM = 28 Å) and in a narrow V continuum filter (λ_c = 5475.3 Å, FWHM = 77 Å), in excellent seeing conditions (as good as $\sim$ 0.4″ during the observations). The detector employed was a CCD TK1024AF with a format of 1024 $\times$ 1024 pixels, which was rebinned by 2 in order to achieve a plate scale of 0.12″ pixel^{-1}. The usual set of bias, dark and flat-field images was acquired together with images of the standard star HD60753 in order to properly calibrate the scientific exposures. Since both nebulae around BE 381 and S 61 were quite faint, images were taken with the central star located both under and outside the occulting mask, to achieve optimal contrast and full spatial coverage of the nebular region.

Table 1. Journal of coronographic and spectroscopic observations

Object	Date	Instrument	Filter or Grating	Slit Position	Exposure Time (s)
S61	01/29/1996	Coron.	Hα		20
S61	”	”	”		300
S61	01/29/1996	EMMI	4	on the star	100+600
S61	”	”	6	”	”
S61	”	”	4	2″ North	2×1000
S61	”	”	6	”	”
S61	”	”	4	2″ South	1000
S61	”	”	6	”	”
S61	07/31/1998	”	6	1″ North	600
S61	”	”	7	”	1200
BE381	01/27/1996	Coron.	Hα		4×100
BE381	”	”	”		5×600
BE381	”	”	”		6×2000
BE381	”	”	V		600
BE381	01/28/1996	EMMI	4	on the star	100
BE381	”	”	6	”	100
BE381	”	”	4	”	2×600
BE381	”	”	6	”	”
BE381	”	”	4	3″ North	1800
BE381	”	”	6	”	”
BE381	”	”	4	3″ South	1800
BE381	”	”	6	”	”

The EMMI spectra were obtained with gratings # 4, # 6 and # 7 which cover the wavelength ranges 3380–5280 Å, 6280–6870 Å and 4520–5820 Å with a spectral resolution (FWHM) of 6.3 Å, 6.3 Å and 2.6 Å, respectively. Two Tektronix CCDs were used: TK2048EB for the EMMI red arm (with a plate scale of 0.27″ pixel^{-1}) and TK1024AB for the blue arm with a plate scale of 0.37″ pixel^{-1}. We employed a longslit of dimensions 1″ by 180″, oriented East - West. We obtained comparison spectra of Ar and HeAr for the wavelength calibration of the gratings, together with detectors bias and flat-field maps. We also observed the standard stars GD108 and Feige110 for the photometric calibration of the spectra. For the observations

of BE 381, we positioned the slit on the star, and at two positions on the nebula, 3″ North and 3″ South respectively. In the case of S 61, we took spectra with the slit on the star and on the nebula, at 2″ North, 1″ North (July 1998) and 2″ South, respectively. We estimate our overall pointing accuracy to be of the order of 1″.

2.2. The data reduction

All data were corrected for bias, flat-fielded, and cleaned to remove cosmic rays and bad pixels using IRAF routines. On the coronographic images, we masked the occulting bar by setting to zero the value of the pixels in the bar region. The spectra were reduced by following the reduction recipe outlined in the IRAF LONGSLIT package. First, the sky background of each frame was modelled with a Chebyshev function of low order into a surface, which was then subtracted from the frame itself. Second, we derived the wavelength calibration in three steps: we identified the emission lines of each comparison spectrum at its central rows and determined the dispersion correction using Chebyshev functions of order between 3 and 4. Then, we re-identified the same emission lines over the entire frame adopting a step of 2 rows and readjusting the dispersion correction at each step. The dispersion corrections obtained in this way were finally fitted into a surface with Chebyshev polynomials of order 6 which was applied to each frame for the final wavelength calibration. Third, we corrected the spectra for atmospheric extinction and calibrated them in flux using the sensitivity functions derived from the standard stars spectrum. We estimate an uncertainty on the resulting fluxes of about 10%.

3. Results

3.1. S 61: the coronographic images

We present the final coronographic Hα image of S 61 nebula in Fig. 1, where North is up and East to the left. This image has been obtained by aligning and adding up all the individual frames, for a total exposure time of 900 s. In this image, we haven't placed the star under the occulting mask, which would otherwise cover a significant portion of the nebula. The apodizing mask within the coronograph suppresses diffraction from the telescope spiders and allows us to achieve good contrast in the nebular region even without using the occulting bar. We find that the S 61 nebula is characterized by a spherical shape with uneven surface brigthness and a mild axisymmetry at the center.

We measure a shell diameter of 7.3″ which translates to 1.8 pc, assuming a distance to the LMC of 51.2 kpc (Panagia et al. 1992). The Hα emission is brightest in a region which peaks about 1.2″ to the north of the star (0.3 pc), and displays a horn shape very similar to the inner nebula resolved around the galactic LBV candidate HD168625 (Hutsemekers et al. 1994; Nota et al. 1996a).

The S 61 nebula is also very reminiscent of the nebula recently discovered around the Ofpe/WN9 star S119 (Nota et al. 1994; Smith et al. 1998). In terms of linear size it is slightly smaller, the S119 nebula is 1.9 × 2.1 pc, and similar to the nebula around the galactic LBV AG Carinae, which is 1.1 × 1.0 pc (Nota et al. 1995).

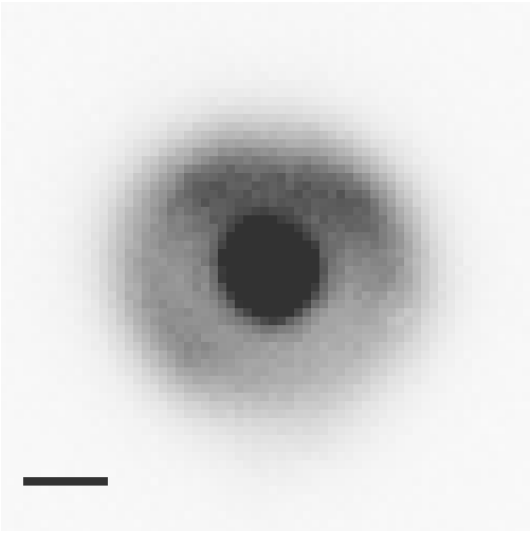

Fig. 1. Coronographic image of the nebula surrounding S 61, taken in the Hα filter. North is up, East at left. In this image, the star is not occulted by the coronographic mask. A scale bar of 1″ is included for reference.

The Hα flux was measured on the image after subtraction of the central source. The reddened Hα flux measured from the image is 1.3×10^{-12} erg s^{-1} cm^{-2}. In order to deredden the nebular measured flux, we have used the value E(B-V) = 0.21, obtained from the spectra (cf. Sect. 3.2). Dereddening the measured Hα flux, we obtain an integrated flux of 2.4 $\times10^{-12}$ erg s^{-1} cm^{-2}.

The mass of ionized gas in S 61 may be calculated from the integrated, extinction free emission line luminosity and electron density. Using the relation:

$$M = 3.87 F_{H\alpha} d^2 T_e^{0.85} \times n_e^{-1}$$

we derive an ionized gas mass of 4.0 M$_\odot$, where n$_e$=400 cm^{-3}, T$_e$=6120 K (cf. Sect. 3.2) and d=51.2 kpc.

3.2. S 61: the spectra

In January 1996, we took spectra in the 3380–5280 Å and 6280–6870 Å bandpasses at three different pointings on the nebula: on the star, and at 2″ North and South respectively. In July 1998 we acquired spectra in the ranges 4520–5820 Å and 6280–6870 Å for the position at 1″ North from the star. The long-slit was aligned East-West, as shown in Fig. 2. We extracted both blue and red spectra for the four observed positions. Extended nebular lines are detected: in the blue region, [OII] λ3726, Hϵ, Hδ, Hγ and Hβ ([NII] λ5755 only at 1″ North), while in the red range [NII] $\lambda\lambda$6548, 6584, Hα and [SII] $\lambda\lambda$6717, 6731. The spectra, extracted by coadding over the spatial extent of the nebular lines, are presented in Fig. 3. Two wavelength regions are displayed: the first is centered on Hα (left panel), and the second includes the HeI λ6678 stellar line and the [SII] $\lambda\lambda$6717, 6731 nebular emissions (right panel). The presence of stellar Hα and HeI λ6678 in the spectra at 2″

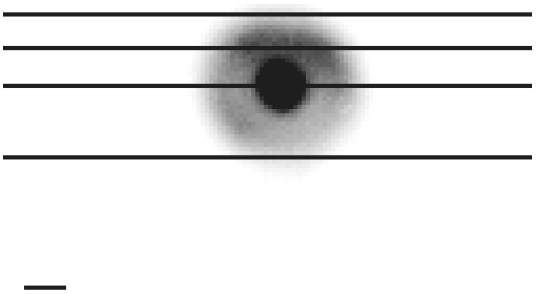

Fig. 2. Coronographic image of the nebula surrounding S 61, on which we have superimposed the four slit positions used in our observations. A scale bar of 1″ is included for reference.

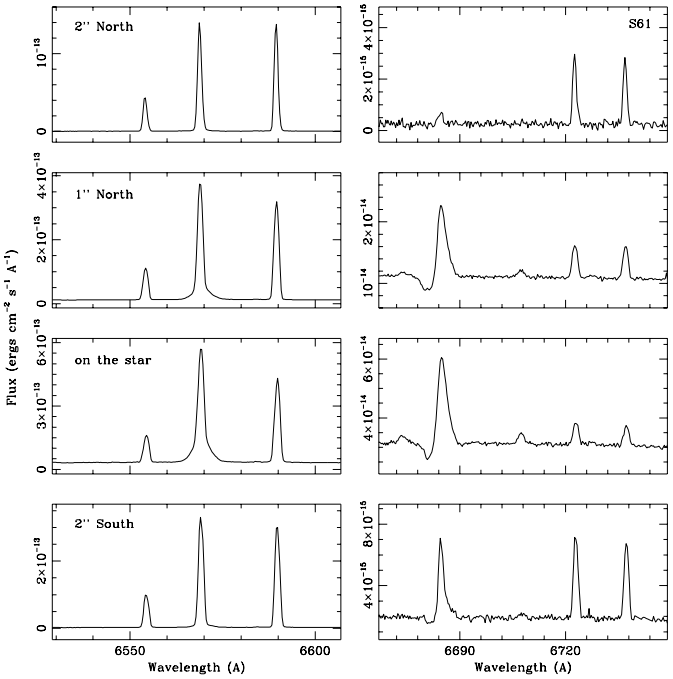

Fig. 3. Spectra of the S 61 nebula for the pointings at 2″ North, 1″ North, on the the central star, and at 2″ South, in the wavelength range from 6530 Å to 6610 Å (left panel) and 6666 Å to 6750 Å (right panel).

North, 1″ North and 2″ South is probably due to contamination from the central star. A strong HeI λ6678 line is present in the pointing at 2″ South, while the line is marginally detected in the pointing at 2″ North.

We used the [NII] λ6584 line to derive the radial velocity map of the nebula. In order to further improve the S/N in the line, we binned the spectrum by a factor of 2 along the spatial direction (corresponding to 0.54″ since 1 pixel = 0.27″), and extracted an individual spectrum from each bin. We measured the peak wavelengths of the [NII] λ6584 line in each extracted spectrum using a multi-gaussian line fitting routine, and derived the radial expansion velocity of the nebula as a function of position with respect to the central star for the pointings on the star and at 2″ North and South, where the S/N ratio is higher. The spectral range between 6280 Å and 6870 Å is characterized by an instrumental line profile of 1 Å FWHM, corresponding to a velocity resolution of 46 km s^{-1}. The observed velocity distributions, referred to the heliocentric system, are plotted in Fig. 4 for the selected slit positions (filled dots). In Fig. 4 we also report the systemic velocity of the star, measured to be 287 km s^{-1} from the HeI λ6678 line. The velocity split in the nebula is well detected in the spectra taken with the slit positioned onto the star and at 2″ South, while only a blueward motion is revealed at 2″ North, located at $\simeq$ 2″ to the East of the star. A comparison with the coronographic image suggests that this motion is possibly representative of the northern, bright arc. We conclude therefore that the nebula is most likely a hollow expanding shell, and in order to derive its kinematical properties, we have fitted the velocity distributions observed on the star and at 2″ South using a simple velocity law derived by Solf & Carsenty (1982) for the case of a spherically expanding shell:

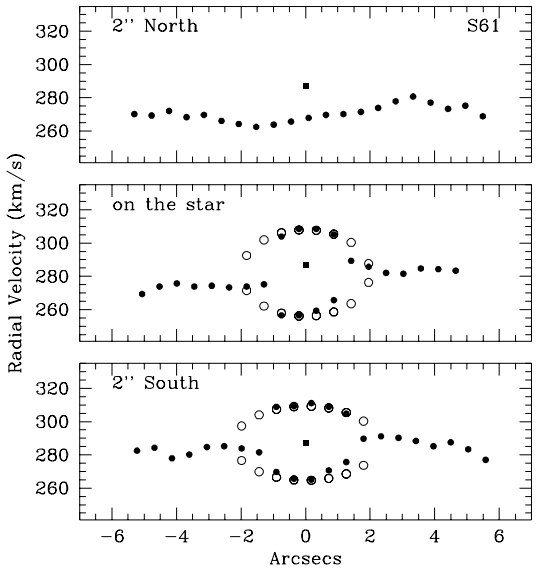

Fig. 4. Radial velocity maps as a function of distance from the star obtained for S 61. From the top to the bottom, the maps correspond to the different pointing positions, namely 2″ North, on the star and 2″ South. Radial velocities are in km s^{-1} while distances are in arcsecs. The filled dots represent the velocity data, and the cross indicates the radial velocity of the star. The open dots are the modelled velocity law for an expanding shell to the velocity distributions observed on the star and at 2″ South (Solf & Carsenty 1982). The fits are centered on the star systemic velocity and have been obtained assuming a nebular radius of 3.6″ and an expansion velocity of 28 km s^{-1}.

$$(V_{\alpha,\delta} - V_0)^2 = V_R^2[R^2 - (\alpha - \alpha_0)^2 - (\delta - \delta_0)^2]/R^2$$

where $V_{\alpha,\delta}$ is the heliocentric radial velocity at the position (α, δ) of our sample and (α_0, δ_0) are the spatial coordinates of the central star. The model is presented in Fig. 4 (open dots) and indicates an expansion velocity of 28 km s^{-1} with a nebular radius of 3.6″. The center of the expansion coincides with the velocity of the star at V_0 = 287 km s^{-1} so that the nebula appears kinematically associated with the central star. From these kinematical properties we infer an age of approximately 30000 yrs, comparable to the dynamical age of the nebulae around R127 (Smith et al. 1998) and S119 (Nota et al. 1995).

Table 2. Observed nebular fluxes for S 61 (in units of 10^{-13} erg s^{-1} cm^{-2})

Lines	2″ N	1″ N	on the star	2″ S
Hβ 4861		1.8		
[NII] 5755		0.014		
[NII] 6548	0.56	1.6	2.2	1.6
Hα 6563	1.9	7.6	14.0	5.7
[NII] 6584	1.8	5.0	7.0	4.9
[SII] 6717	0.036	0.095	0.13	0.084
[SII] 6731	0.033	0.090	0.12	0.078

Table 3. Deblended stellar and nebular fluxes in Hβ and Hα lines (in units of 10^{-13} erg s^{-1} cm^{-2}) for S 61

Lines	Source	2″ N	1″ N	on the star	2″ S
Hβ	star		0.33		
	nebula		1.6		
Hα	star	0.094	1.7	5.5	0.46
	nebula	1.9	6.1	10.0	5.5

In addition to the kinematical properties, the nebular emission lines provide information on the physical and chemical characteristics of the nebula. Unfortunately, the spectra obtained in 1996 with EMMI in the blue region could not be reliably flux calibrated: therefore, we list in Table 2 the observed line fluxes of only the red spectra taken in 1996 and the line fluxes of both blue and red spectra, obtained in 1998. We have deblended the stellar and nebular contributions to the Hβ and Hα lines observed for each slit position by using a multigaussian fit. The resulting individual stellar and nebular fluxes are listed in Table 3. The accuracy of the fitting procedure is estimated to be $\simeq 5\%$, and well within the uncertainty of the flux calibration. Following Osterbrock's notation for Case B recombination, and assuming an electron temperature T_e = 5000 K, which well approximates the nebular physical conditions, we have used the Hα/Hβ ratio to calculate the extinction coefficient cβ at the 1″ North position. We have obtained cβ = 0.33. In order to derive from this value the reddening E(B-V), we have fitted the cβ and corresponding E(B-V) values reported in Table 3 of Kaler & Lutz (1985) with a polynomial of second order. The fit gives an E(B-V) value of 0.21 which fairly agrees with the E(B-V) = 0.15 obtained by Pasquali et al. (1997) from the comparison between model atmospheres and the observed spectral energy distribution of S 61.

We have measured the N^+/S^+ ratio in order to qualitatively evaluate the nitrogen abundance in S 61. The values are in the last column of Table 4 and range between 34 and 40, with a mean of 36 ± 3. In this respect, S 61 nebula closely resembles R127 (also in Table 5) and P Cygni at $N^+/S^+ = 33 \pm 5$ (Johnson et al. 1992) and, therefore, it is nitrogen enriched at the same extent of other LBV nebulae. A more detailed chemical analysis relies on the electron temperature and density of the nebula. First, we have scaled the line fluxes measured at 1″ North to Hβ = 100, and dereddened them using cβ = 0.33 (cf. Table 4). Second, we have used the [SII]6717/6731 ratio to determine n_e and the ([NII]6548+6584)/[NII]5755 ratio to evaluate T_e. With the IRAF package NEBULAR (TEMDEN routine) we have derived T_e = 6120 K and n_e = 400 cm^{-3}. Finally, we have calculated the ionic abundance from each N and S line using the IONIC routine in the same package. The ionic abundances obtained for each element have been scaled by the corresponding line fluxes and added up to derive the total element abundance. Table 5 summarizes the final N and S abundances obtained for the position at 1″ North in units of Log(X/H) + 12 and compares them to the abundances derived for two established LBVs (AG Car and R127), one Ofpe/WN9 (S119), and to the mean abundances found for HII regions. In the case of S119, we have listed two sets of abundances, derived assuming T_e = 5600 K (first row) and T_e = 6800 K (second row). These two values are reported from the ionic abundances calculated by Smith et al. (1998) due to the non-detection of the [NII] λ5755 line. Within the uncertainty of about 0.2 dex in the chemical composition, we may conclude that S 61 nebula not only is very similar to S119 but also matches the typical properties of LBV nebulae, by having a N overabundance of $\sim$ 1 dex and a S underabundance of $\sim$ 0.5 dex with respect to a typical HII region.

Table 4. Dereddened line fluxes for the 1″ North position, in units of Hβ = 100 erg s^{-1} cm^{-2}

Line	Flux
[NII] 5755	0.7
[NII] 6548	76.7
Hα	323.7
[NII] 6584	242.0
[SII] 6717	4.6
[SII] 6731	4.3

Table 5. S 61 nebular abundances, compared to other LBVs, in units of Log(X/H) + 12

Object	N/H	S/H	N/S
S61 1″ N	8.48	6.35	35
S61 2″ N			34
S61 2″ S			40
AG Car[1]	8.22	>6.56	<46
R127[2]	8.05	6.52	34
S119[2]	8.08	6.18	36
	8.41	6.52	36
HII region[3]	7.57	7.06	3

(1) Smith et al. 1997 (2) Smith et al. 1998 (3) Shaver et al. 1983

3.3. BE 381: the coronographic images

In Fig. 5 we show the final Hα image of the region around BE 381 with North up and East to the left. For this observa-

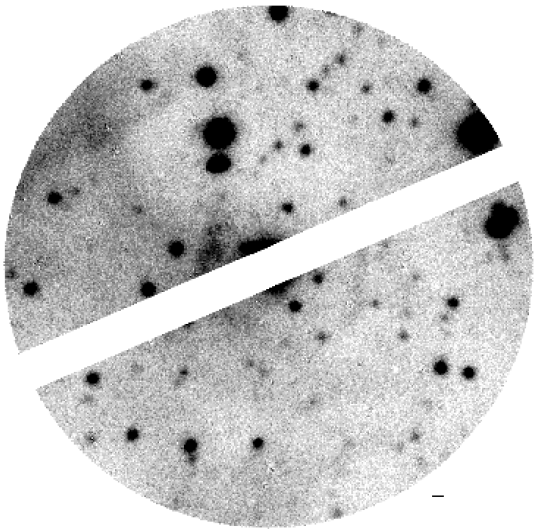

Fig. 5. Coronographic image of BE 381 circumstellar region in the light of Hα (North is up and East left) with the star occulted by the coronograph bar. A scale bar of 1″ is included for reference.

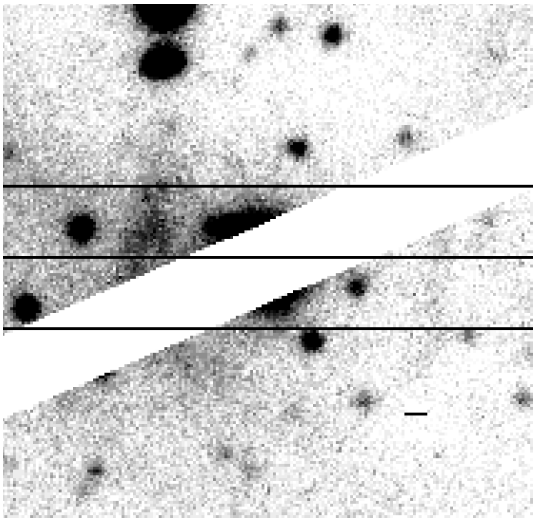

Fig. 6. Observed slit positions projected on the coronographic image of BE 381 (North is up, East left). From the top: 3″ North, on the star and 3″ South. A scale bar of 1″ is included for reference.

tion, the central star has been placed under the coronographic wedge, to achieve maximum enhancement of the circumstellar surroundings. It is evident from the figure that BE 381 lies in a diffuse HII region which appears denser at the NE and to the SE. Two diffuse arches in the image suggest the possibility of a shell structure around BE 381. The exact nature of these two structures is not clear, however, since the eastern component may be associated with the extended diffuse nebulosity seen towards the NE. The arches define a shell of diameter 13″ which translates into $\sim$ 3.2 pc at the LMC distance of 51.2 kpc (Panagia et al. 1992), with the structure to the east of BE 381 being much brighter than the western arch. The star appears to be located slightly offcenter with respect to the two arches, at a distance of 6″ (1.3 pc) from the eastern arch, and of 7″ (1.8 pc) from the western arch.

3.4. BE 381: the spectra

Fig. 6 shows the observed slit positions projected on the image of BE 381. Because of the poor S/N ratio achieved in the blue spectral region, we have analysed only the spectra taken in the region 6280–6870 Å. In these longslit spectra, we detect the nebular lines of [NII] $\lambda\lambda$6548, 6584, Hα and [SII] $\lambda\lambda$6717, 6731. In the spectrum centered on the star, we detect strong stellar HeI λ6678 emission (Fig. 7). The integrated line fluxes (not corrected for reddening) are listed in Table 6. The nebular lines of [NII] and [SII] are spatially extended. The emission is stronger in correspondence with the brighter eastern arch, and it extends up to $\simeq$ 14″ (3.5 pc) from the star. On the western side of the star the emission is rather faint and seems to extend over $\simeq$ 9″ (2.1 pc).

We have used both the Hα and [NII] λ6584 lines to derive the kinematical information. In order to improve the S/N in our data, we have binned the spectrum by 4 pixels (1″), along the

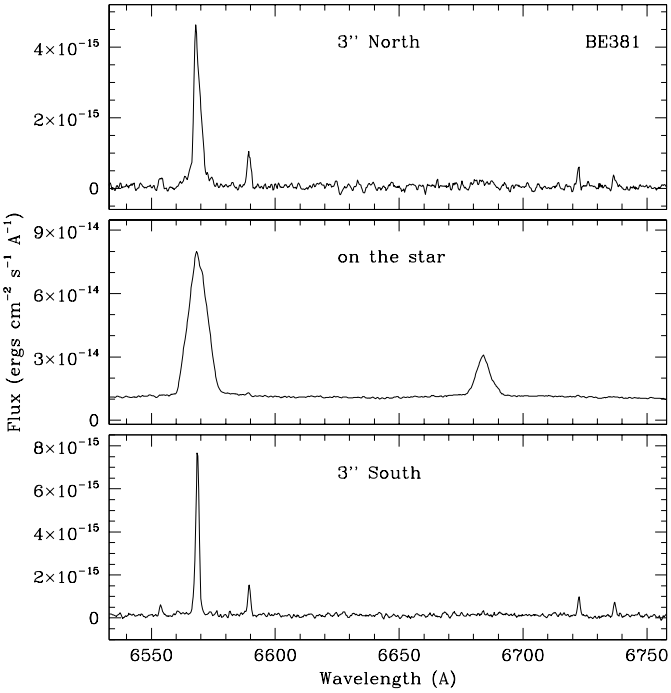

Fig. 7. Spectra of the BE 381 nebula for the pointings at 3″ North, on the the central star, and at 3″ South, in the wavelength range between 6530 Å and 6760 Å.

Table 6. Observed nebular fluxes for BE 381 (in erg s^{-1} cm^{-2})

Lines	3″ N	on the star	3″ S
[NII]λ6548	6.0×10^{-16}		7.1×10^{-16}
[NII]λ6584	1.8×10^{-15}	2.1×10^{-15}	2.0×10^{-15}
[SII]λ6717	6.2×10^{-16}	1.1×10^{-15}	1.0×10^{-15}
[SII]λ6731	4.3×10^{-16}		7.6×10^{-16}

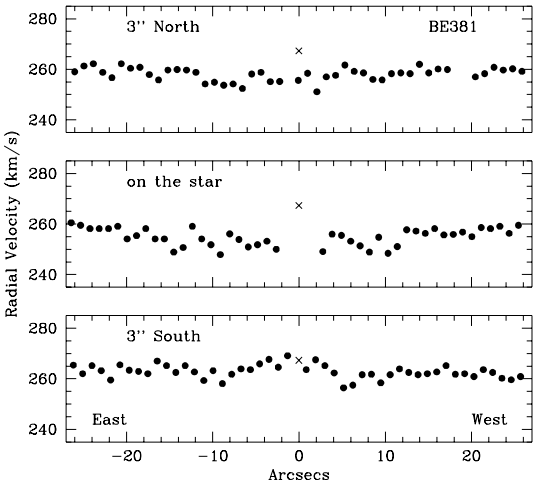

Fig. 8. Radial velocity map of BE 381 as a function of distance from the star. The radial velocities are reduced to the heliocentric frame of reference. They are plotted, in units of km s^{-1}, as a function of position (in arcseconds) with respect to the star. The cross indicates the radial velocity of the star.

spatial direction and extracted the binned spectra. We have measured both Hα and [NII] λ6584 peak wavelength, and calculated their corresponding radial velocities, which have then been referred to the heliocentric system of reference and averaged. The values derived from the two different lines were averaged; the mean standard deviation associated with the averaged velocities is small ($\sim$ 3 km s^{-1} with a peak standard deviation of 6 km s^{-1}), and well within the spectral resolution of 46 km s^{-1} of our observing configuration.

The averaged radial velocities are plotted as a function of position with respect to the star in Fig. 8 for the pointings at 3″ North, on the star, and 3″ South (filled dots). In the figure, the cross represents the star radial velocity, which has been determined to be 267.3 km s^{-1} from the average of the Hα and HeI λ6678 lines. The data are characterized by a resolution of FWHM = 1 Å, corresponding to a velocity of 46 km s^{-1} at Hα. No velocity structure is present in the pointings at 3″ North or South; both distributions are flat, averaged around 258 $\pm$ 3 km s^{-1} and 263 $\pm$ 3 km s^{-1}, respectively, possibly indicating the overall motion of the underlying interstellar region. In the map obtained with the slit on the star there appears to be a mild distortion to the otherwise flat distribution, between 20″ to the east and 10″ to the west, which may be interpreted as a blueward motion of the region surrounding BE 381 with a velocity $\sim$ 20 km s^{-1} with respect to the star.

Within the errors, this result is in broad agreement with Nota et al. (1996b) who suggested the presence of two different velocity components in the Hα profile of BE 381, obtained with high resolution echelle spectroscopy. These components were believed to be the signature of a shell expanding at about 30 km s^{-1}. Given the lower spectral resolution of our data compared to Nota et al. (1996b) it is plausible that we do not resolve the second component but just detect the overall motion.

In addition to the kinematics, from the nebular spectra we can also derive some basic chemical information: we have measured the [SII] 6717/6731 ratio for positions 3″ North and 3″ South in order to estimate the gas density. We have assumed an electron temperature T_e = 10000 K, and we have derived (using the IRAF NEBULAR package) a mean density of $\sim$ 30 cm^{-3} and 120 cm^{-3} at 3″ North and South, respectively. It is interesting to notice that Nota et al. (1996b) estimated a gas density of 800 cm^{-3} from the [SII] lines in the echelle spectrum taken on the star. For their echelle measurements, they used a slit of size 1.″5 $\times$ 5″, which most likely missed both nebular arches. Their density measurements therefore refer to a circumstellar region very close to the star. We have searched for [SII] emission in the spectrum taken with the slit centered onto the star in order to resolve this apparent discrepancy, but the contamination from the stellar source is large and no [SII] lines are detected at that position.

We have also extracted from the longslit frames the brightest nebular region, corresponding to the eastern arch and repeated the analysis. We find that the eastern circumstellar region is not homogeneous: the gas density varies from 120 cm^{-3} at 3″ N to 240 cm^{-3} at 3″ South. Unfortunately, the low S/N ratio of the spectra does not allow us to determine the gas density of the fainter arch to the west of BE 381. Since the nebular Hβ flux is not available and the Hα flux is strongly contaminated by the stellar wind, we are not able to derive exact chemical abundances for the nebula around BE 381. Nevertheless, we can use the N^+/S^+ ratio to establish the nebular content of nitrogen. We have obtained a mean N^+/S^+ ratio of 2.3 at 3″ North and 1.5 at 3″ South, respectively. For the eastern circumstellar region alone the ratio N^+/S^+ results to be 1.9 in the North position and 1.2 in the South. These values are comparable, within the errors, to the averaged N^+/S^+ ratio of 3 derived for classical HII regions by Shaver et al. (1983). Alternatively, ejected nebulae such as LBV nebulae are characterized by N^+/S^+ value ranging between 33 (i.e. P Cygni, Johnson et al. 1992) and 80 (HR Carinae, Nota et al. 1997). Therefore, we may rule out a stellar origin for the shell surrounding BE 381.

Table 7. The sample of LMC Ofpe/WN9 from Pasquali et al. (1997)

S/R/BE	HD/HDE	Sk	IRAS/Brey
S9		−66D40	
S91/R84/BE543	269227	−69D79	Brey 18
S30/R99/BE261	269445	−68D73	
BE294	269582	−69D142a	
S119/BE335	269687	−69D175	IRAS 05317−6907
	269927c	−69D249c	Brey 91
BE381			Brey 64
S61/BE153		−67D266	

4. Discussion and conclusions

Out of the original sample of 8 LMC Ofpe/WN9 stars originally investigated by Nota et al. (1996b), and Pasquali et al. (1997) and listed in Table 7, five have been found to have nebular lines in their ground based optical spectra (see also Walborn, 1982;

Table 8. Optical and Near-IR photometry from Nota et al. (1996). Stellar properties from Pasquali et al. (1997)

	S119	S61
U	10.86	10.93
B	11.83	11.88
V	11.90	12.01
J	11.73	12.03
H	11.65	12.02
K	11.58	11.88
T_*(K)	30900	36100
$R_*(R_\odot)$	35	28
$\log(L/L_\odot)$	6.0	6.1
M ($M_\odot$ yr^{-1})	2.7×10^{-5}	2.2×10^{-5}
H/He by mass	0.31/0.69	0.33/0.67

Bohannan & Walborn 1989). These five stars were the subject of subsequent detailed studies aimed at establishing whether the nebular lines were indication of the presence of an associated ejected nebula.

As already mentioned, the nebula around BE 381 has been found to be kinematically associated, but not composed of ejected material, and therefore has most likely been formed by interstellar medium swept up by the fast O stellar wind. Very little can yet be said of either R99 or HDE269927c. Attempts were made to resolve a circumstellar nebula around R99 from the ground with coronography, and with HST (Schulte-Ladbeck et al. 1998), and have failed so far. HDE269927c has also been investigated from the ground with coronography without a detection, and HST observations are still pending (Schulte-Ladbeck et al. 1998). We can safely conclude that out of the original sample, only S119 and S 61 show convincing evidence of an associated circumstellar nebula composed of ejected material.

From the point of view of the stellar properties, S119 and S 61 are quite similar, in terms of terminal wind velocity, luminosity and mass loss rate. In Table 8, extracted from Pasquali et al. (1997), we list their fundamental parameters, derived from HST UV and optical spectroscopic observations: with the possible exception of the temperature, which places the two stars roughly at the two extremes of the Ofpe/WN9 sequence, all parameters are very similar. Neither star is known to be variable: however, very few observations have been obtained for these two stars in recent years, and any possible variability could have been missed.

The two associated nebulae are also very similar, in terms of morphology, size, and kinematical characteristics. Their morphology is an elliptical shell, with well defined boundaries. A very bright lobe can be distinguished in both nebulae, at PA $\simeq$ = 45^o for S119 (Nota et al. 1994), and PA = 0^o for S 61. They have roughly the same nebular spatial extension: $7.7'' \times 8.6''$ for S119, corresponding to a linear scale of 2×2 pc, $7.3''$ in diameter for S 61 (1.8 pc). The two nebulae expand with velocities which, within the errors, are identical: 25 km s^{-1} for S119, 28 km s^{-1} for S 61. Hence, the dynamical ages are also very similar: 5×10^4 yrs for S119, 3×10^4 yrs for S 61. In terms of mass, S 61 (4 $M_\odot$) is a factor of two more massive than S119 (1.7 $M_\odot$, Nota et al. 1994), mainly due to a difference in density. In fact, Smith et al. (1998) find for S119 an upper limit to the T_e of 6800 K, and a corresponding density of n_e = 680, in correspondence to the brightest lobe of the nebula. In comparison, we find for S 61 a value n_e = 400 and T_e = 6120 K at the pointing position $1''$ N. However, it is necessary to point out that when we calculate the mass of ionized gas contained in the nebula, we assume an average density. Significant density variations have been noticed in the S119 nebula (Nota et al. 1996b), possibly indicating that the nebula is clumpy, and the determination of the mass might be affected by a high uncertainty. In addition, in order to determine the density, we use the [SII] 6717/6731 ratio in a regime where a small variation in the ratio (10%) can produce a large difference in the determination of the density (a factor two) and, therefore, of the mass.

We can conclude that within the limitations associated with our measurements, S119 and S 61 are in a very similar phase of their evolutionary history. The presence of an ejected nebula also indicates that they have undergone, some 10^4 yrs ago, a LBV type *"giant outburst"* where they have ejected a significant fraction of their outer layers in the surrounding medium. We can confidently state this was a *true* LBV outburst because in both cases the ejected nebulae are also very similar to typical LBV nebulae, such as AG Carinae, in terms of morphology, size, dynamical ages and masses.

Moreover, the similarity extends to the chemical composition, and we do find for these two Ofpe/WN9 ejected nebulae the same abundance anomaly recently found for a number of galactic and LMC LBVs (eg. AG Carinae; Smith et al. 1997). The chemical composition of the nebula around S119 had been already derived by Smith et al. (1998), who used HST/FOS spectra of the brightest nebular region to derive nebular parameters and element abundances. They were not able to derive a secure value for the electron temperature, but with an upper limit of 6800 K they derived N/O = 1.41–2.45, N/H = 8.08–8.41, S/H = 6.18–6.52. They compared the nebular abundances obtained with the expected surface abundances of LBVs and concluded that, if LBV atmospheres consist of CNO-processed material, the event which generated the nebula had taken place before, or at the very start, of the LBV phase. Comparison of these nebular abundances with the abundances, for example, of SN1987A, showed remarkable similarity. The inner ring of SN1987A is thought to be composed of RSG wind material (Fransson et al. 1989; Panagia et al. 1997). This finding, together with other considerations on the nebular expansion velocities, and on the dust content (Waters 1998), suggest that LBV nebulae were once the CN-processed convective envelope of a RSG. For S 61, we also find high N enrichment, comparable to S119. We conclude that such enrichment is also consistent with material which has been CN-processed only, as observed in PN. However, a detailed abundance analysis will be necessary to put on firm quantitative grounds our findings and to establish whether there is any O depletion. The slow expansion velocity of the nebula would also support the RSG origin.

Our new findings on the element abundances for S 61 have a threefold impact:

1) they complement the morphological and kinematical information in establishing a close similarity between the two nebulae around S119 and S 61. This similary is especially interesting considering that these are the *only* two confirmed associated nebulae around Ofpe/WN9 stars discovered so far, and it implies that not only these two stars have undergone a LBV type outburst, but the nebular composition confirms that this event has occurred approximately at the same time in their evolution;

2) together with the morphological and kinematical information, they add one more point in support to the scenario that Ofpe/WN9 stars are closely related to LBVs. In fact, the measured N/S and N/H ratios for the S 61 nebula (Table 5) are in very good agreement with results already obtained on LBV nebulae such as AG Carinae (Smith et al. 1997) and R127 (Smith et al. 1998), also reported in Table 5.

3) They also support the suggestion by Smith et al. (1998) that these nebulae most likely were the convective envelope of a RSG, which has been gently shed prior to the classical LBV phase.

In order to understand whether this scenario is correct, more work is needed both on the observational and theoretical aspects of the problem. Observationally, it is necessary to perform accurate abundance analyses of all LBV nebulae, and therefore establish accurately the statistical significance of these findings. Theoretically, a consistent evolutionary scenario is needed which explains how these superluminous stars can experience a RSG phase when no such luminous RSG counterpart is actually observed.

Acknowledgements. We are grateful to the ESO Observatory for their support of the STScI Coronograph project, and we thank Colin Cox, Knute Ray, Bruce Douglas for the technical support. We are indebted to Francesco Paresce, Chris Burrows and Massimo Robberto for their contributions to the Coronograph development. We would like to thank the referee Dr. S. Pineault for invaluable remarks.

References

Bohannan B., Walborn N.R., 1989, PASP 101, 520
Clampin M., Paresce F., Robberto M., 1994, SPIE 2198, 172
Conti P.S., 1984, In: Maeder A., Renzini A. (eds.) IAU Symp. 105, Observational Test for Stellar Evolution Theory. Reidel, Dordrecht, p. 233
Crowther P.A., Hillier D.J., Smith L.J., 1995, A&A 293, 172
Davidson K., 1987, In: Lamers H.J.G.L.M., de Loore, C. (eds.) Instabilities in Luminous Early Type Stars. Kluwer, Dordrecht, p. 127
Fransson C., Cassatella A., Gilmozzi R., et al., 1989, ApJ 336, 429
Hubble E., Sandage A., 1953, ApJ 118, 353
Hutsemekers D., van Drom E., Gosset E., Melnick J., 1994, A&A 290, 906
Johnson D.R.H., Barlow M.J., Drew J.E., Brinks E., 1992, MNRAS 255, 261
Kaler J.B., Lutz J.H., 1985, PASP 97, 700
Maeder A., 1989, In: Davidson K., Moffat A.F.J., Lamers H.J.G.L.M. (eds.) IAU Coll. 113, Physics of Luminous Blue Variables. Kluwer, Dordrecht, p. 15
Morris P.W., Eenens P.R.J., Hanson M.M., Conti P.S., Blum R.D., 1996, ApJ 470, 597
Nota A., Drissen L., Clampin M., et al., 1994, In: Clegg R., et al. (eds.) Circumstellar Media in the Late Stages of Stellar Evolution. Cambridge University Press, Cambridge, p. 89
Nota A., Livio M., Clampin M., Schulte-Ladbeck R., 1995, ApJ 448, 788
Nota A., Pasquali A., Clampin M., et al., 1996a, ApJ 473, 946
Nota A., Pasquali A., Drissen L., et al., 1996b, ApJS 102, 383
Nota A., Smith L.J., Pasquali A., Clampin M., Stroud M., 1997, ApJ 486, 338
Panagia N., Gilmozzi R., Kirshner R.P., Pun C.S.J., Sonneborn G., 1997, Bull. American Astron. Soc. 191, 1909
Panagia N., Gilmozzi R., Macchetto F., Adorf H.-M., Kirshner R.P., 1992, ApJ 380, L23
Pasquali A., Langer N., Schmutz W., et al., 1997, ApJ 478, 340
Schulte-Ladbeck R.E., et al., 1998, in preparation
Shaver P.A., McGee R.X., Newton L.M., Danks A.C., Pottasch S.R., 1983, MNRAS 204, 53
Smith L.J, Nota A., Pasquali A., et al., 1998, ApJ, 503, 278
Smith L.J., Crowther P.A., Prinja R.K., 1994, A&A 281, 833
Smith L.J., Stroud M.P., Esteban C., Vílchez J.M., 1997, MNRAS 290, 265
Solf J., Carsenty U., 1982, A&A 116, 54
Stahl O., 1986, A&A 164, 321
Stahl O., Wolf B., Klare G., et al., 1983, A&A 127, 49
Walborn N.R., 1982, ApJ 256, 452
Waters L.B.F., 1998, In: Wolf B., et al. (eds.) IAU Coll. 169, Variable and Non-spherical Stellar Winds in Luminous Hot Stars. in press